Available online at www.sciencedirect.com
SCIENCE DIRECT®
ELSEVIER
Earth and Planetary Science Letters 219 (2004) 377–396
EPSL
www.elsevier.com/locate/epsl

Geomagnetic moment variation and paleomagnetic excursions since 400 kyr BP: a stacked record from sedimentary sequences of the Portuguese margin ☆

Nicolas Thouveny [a,*], Julien Carcaillet [a], Eva Moreno [a], Guillaume Leduc [a], David Nérini [b]

[a] *CEREGE, Europôle Méditerranéen de l'Arbois, P.O. Box 80, Aix en Provence Cedex 4, France*
[b] *Centre d'Océanologie de Marseille, Case 901, Luminy, 13288 Marseille Cedex 9, France*

Received 23 December 2002; received in revised form 26 November 2003; accepted 4 December 2003

Abstract

A paleomagnetic study was performed in clayey-carbonate sedimentary sequences deposited during the last 400 kyr on the Portuguese margin (Northeast Atlantic Ocean). Declination and inclination of the stable remanent magnetization present recurrent deviations from the mean geomagnetic field direction. The normalized intensity documents a series of relative paleointensity (RPI) lows recognized in other reference records. Three directional anomalies occurring during RPI lows chronologically correspond to the Laschamp excursion (42 kyr BP), the Blake event (115–122 kyr BP) and the Icelandic basin excursion (190 kyr BP). A fourth directional anomaly recorded at 290 kyr BP during another RPI low defines the 'Portuguese margin excursion'. Four non-excursional RPI lows are recorded at the ages of the Jamaica/Pringle Falls, Mamaku, Calabrian Ridge 1, and Levantine excursions. The RPI record is characterized by a periodicity of ~100 kyr, paleointensity lows often coinciding with the end of interglacial stages. This record sets the basis of the construction of an authigenic $^{10}Be/^{9}Be$ record from the same sedimentary sequences [Carcaillet et al., this issue].

Keywords: sedimentary records; geomagnetic field directions and paleointensity; paleomagnetic excursions; paleomagnetic events; relationships between the climate and the geomagnetic field

1. Introduction

Among the paleomagnetic excursions or events of the Brunhes normal polarity chron (e.g. [2,3]), only a few were recorded in volcanic rocks and were accurately dated. The recognition of such paleomagnetic anomalies in sedimentary records is delicate because, according to sediment properties and accumulation rates, the geomagnetic vector deviations can be recorded under various

* Corresponding author. Tel.: +33-442-97-1558; Fax: +33-442-971595.
E-mail address: thouveny@cerege.fr (N. Thouveny).

☆ Supplementary data associated with this article can be found at doi:10.1016/S0012-821X(03)00701-5

0012-821X/04/$ – see front matter © 2004 Elsevier B.V. All rights reserved.
doi:10.1016/S0012-821X(03)00701-5

forms, from large amplitude paleosecular variation to abrupt full reversals. Few studies even revealed recurrent and lasting reversed events during the Brunhes chron (e.g. [4]). The reliability of normalized intensity records as relative paleointensity (RPI) proxies is also questionable. A first order similarity between independent RPI records justified the construction of regional [5] or global [6] stacks, but high resolution RPI reconstructions from high sedimentation rate environments are still necessary. The present article presents the construction of a new high resolution paleomagnetic record for the last 400 kyr that will be compared with the authigenic $^{10}Be/^{9}Be$ ratio record constructed from the same cores [1].

2. General setting and chronology of the sequence

Giant piston cores and gravity cores were collected on the Portuguese margin (Fig. 1) by the French R.V. *Marion Dufresne* in the framework of the IMAGES program (IGBP-PAGES). During IMAGES 1 (1995), three giant cores were collected in two areas: (1) cores MD95-3039 (35.2 m long) and MD95-2040 (35.7 m long) at ca. 40°35′N, on the western and eastern slopes of the Oporto Seamount, at depths of 3380 m and 2465 m, respectively; (2) core MD95-2042 (39.6 m long) at ca. 37°48′N, at 3146 m depth, in a flat area of the continental rise. During IMAGES V leg V (1999) and Geociences (2001), cores MD99-2334K, MD01-2440G and MD01-2441 (5, 7 and 14 m long, respectively) were collected with short and light gravity corers on the site of core MD95-2042.

Beneath beige-pink oxidized carbonate ooze, the sedimentary sequences are composed of pelagic light-gray clayey mud, deposited under glacial conditions, alternating with beige clayey-carbonate ooze deposited under interglacial conditions [7–10]. Thin layers of significantly larger grain size recognized as ice-rafted debris (IRD) were identified to Heinrich or Heinrich-like events [9,10].

Radiocarbon ages are available from core SU81-18 [11] and from core MD95-2039 [12]; they were corrected for a standard reservoir effect

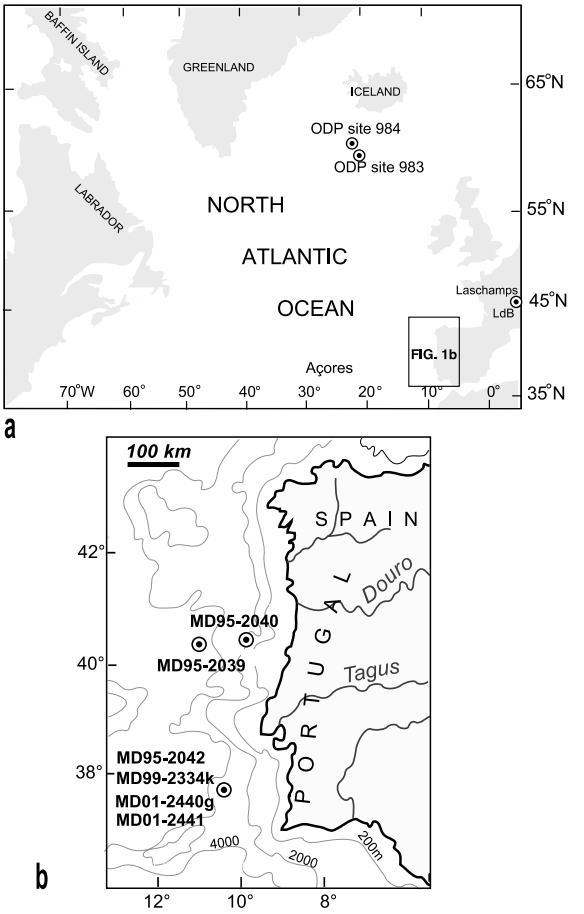

Fig. 1. Geographic location of the studied cores and other key sites. A map of the northern area of the North Atlantic ocean with surrounding continents (a) is completed by a map of the studied area with coring sites locations (b).

of 400 years and calibrated using the equation of Bard [13] (Table 1). Average ages of Heinrich event 3 (31.2 kyr BP) and Heinrich event 4 (39.4 kyr BP) [9] provide complementary chronological constraints between 30 and 40 kyr BP. The benthic $\delta^{18}O$ records of core MD95-2039 [12] and MD95-2042 ([14,15] and unpublished results) document marine isotopic stages (MIS) 1–9 and 1–6, respectively. A correlation to astronomically dated reference curves [16,17] provides the age series (Table 1).

A correlation matrix based on numerous susceptibility markers (e.g. fig. 2 in [10]) helped to transfer all available chronological data from

core to core, providing a complete chronological data set applicable to all studied cores. New radiocarbon determinations on MD95-2042 (E. Bard, personal communication) and $\delta^{18}O$ records of MD95-2040 ([18] and De Abreu, personal communication) confirm the validity of the chronological data sets used here.

Depth to time transfer was performed for each core using a polynomial best fit ($r > 0.99$) computed through available ages (Fig. 2). The deepest layer located at 35 m in core MD95-2040 is dated by extrapolation at 400 kyr BP. Successive time intervals (0–60 kyr BP, 60–160 kyr BP, 160–350 kyr BP and 350–400 kyr BP) are covered by six, three, two and one cores, respectively. In the southern area (e.g. core MD95-2042), *apparent* sedimentation rates vary from 15 to 35 cm/kyr. In the northern area (cores MD95-2039 and MD95-2040), *apparent* sedimentation rates vary from 7 to 25 cm/kyr.

3. Rock magnetism and determination of magnetic carriers

Standard 8 cm^3 specimens and/or 1.5 m long U-channels of 4 cm^2 section were collected along the studied cores. Low field magnetic susceptibilities were measured on a KLY2 Kappabridge. The susceptibility was normalized to the sediment mass and expressed as mass-specific susceptibility χ. The remanent magnetization was measured using two generations of a 2G superconducting rock magnetometer 760R: the RF SQUIDs version (diameter = 120 mm) for specimens, and, since 1999, the DC SQUIDs version (diameter = 45 mm) for U-channels and complementary specimens. A Schonstedt GSD-1 demagnetizer and the 'in-line' 2G coil sets were used for AF demagnetization. Isothermal remanent magnetizations (IRM) were imparted by placing specimens in pulsed magnetic fields of 0.3, 1.0 and 2.8 T, or by passing U-channels through permanent magnets providing fields of 0.3 and 1 T, respectively [19]. Anhysteretic remanent magnetizations (ARM) were imparted in a 0.1 mT bias field combined with a linearly decaying alternating field of 100 mT.

Scanning electron microscopy and X-ray energy dispersion analyses in agreement with hysteresis parameters and Curie temperatures (see supplementary Figs. 1 and 2[1]) identify the main magnetic carriers as single domain (SD), pseudo-single domain (pSD) and multi-domain (MD) titanomagnetite. Average values of the M_r/M_s and H_{cr}/H_c ratios [20] were computed for different clusters representing several sedimentary facies; they plot, as in most sediment mixtures, in the pSD area, with a bias towards the MD area for IRD layers (see supplementary Fig. 3a[1]). The distribution of χ_{ARM} versus χ [21] suggests that grain sizes are < 1 μm in glacial and interglacial sediments and reach 5 μm in IRD layers (see supplementary Fig. 3b[1]). Glacial clays and interglacial clayey-carbonate ooze can be further distinguished by different magnetic grain sizes documented by different χ_{ARM}/χ ratios (see supplementary Fig. 3b[1]). It must be stressed that this method of grain size determination [21], valid for pure magnetite samples, underestimates the titanomagnetite grain sizes.

Variations of rock magnetic parameters were interpreted in terms of environmental and climatic variations [9,10]. Numerous χ and IRM peaks identify thin IRD layers containing a coarse fraction of Ti-magnetite and silicates transported during Heinrich events by residual iceberg masses [9]. On a longer term, χ_{ARM}, χ_{ARM}/χ and ARM/IRM evidence magnetic grain size variations tightly linked to glacial–interglacial alternations. Nevertheless, these sedimentary sequences, after rejection of IRD layers, present a homogeneity in composition and granulometry appropriate for reconstructing paleomagnetic directions. Since they also respect criteria of uniformity in concentration and grain size [22], they should enable the reconstruction of variations of the RPI.

4. Sedimentary magnetic fabric

The anisotropy of magnetic susceptibility was used to check the sedimentary fabric (e.g. [23,24]) and to assess the reliability of paleomag-

[1] See the online version of this article.

Table 1
Chronological data obtained on cores SU81-18 [11], MD9520-39 [12], MD95-2042 [14,15]

Core	Depth (cm)	Depth of MD95-2042 (cm)	^{14}C age −400 years reservoir correction	Calibrated age (yr BP)	Error (years)
SU81-18 [11]	90	204.82	5 240	5 971	140
SU81-18	111	236.83	6 790	7 660	140
SU81-18	130	266.49	7 590	8 489	120
SU81-18	141	283.86	8 760	9 756	130
SU81-18	150	298.15	9 360	10 486	130
SU81-18	180	345.97	10 280	11 934	140
SU81-18	190	361.91	10 680	12 424	140
SU81-18	200	377.81	11 010	12 828	170
SU81-18	209	392.08	11 760	13 744	200
SU81-18	230	425.16	12 260	14 353	170
SU81-18	250	456.31	12 460	14 596	150
SU81-18	260	471.74	12 700	14 887	170
SU81-18	280	502.29	13 580	15 952	190
SU81-18	299	530.91	13 950	16 399	180
SU81-18	310	547.3	14 490	17 049	230
SU81-18	330	576.78	14 590	17 169	190
KIA780/G.b. [12]	168.5	419.97	12 220	14 304	110
KIA781/G.b.	208.5	480.58	13 120	15 396	100
KIA782/N.p.	208.5		13 530	15 892	100
KIA785/G.b.	542.5	839.29	19 740	23 278	210
KIA786/N.p.	542.5		20 320	23 956	220
KIA787/G.b.	648	968.19	22 410	26 382	280
KIA788/G.b.	818.5	1 160.13	27 580	32 271	520
Isotope stage (upper limit)	MIS limits in core MD95-2039 depth (benthic δ^{18}O) [12]	MIS limits in core MD95-2042 depth (benthic δ^{18}O) [14]	Age (a) from [16,17]		
4		1 822.31	59 000		
5	1 550.0	1 976.95	74 000		
5.1	1 660.0	2 123.28	79 000		
5.2	1 710.0	2 196.55	91 000		
5.3	1 760.0	2 278.65	100 000		
5.4	1 850.0	2 432.05	111 000		
5.5	1 900.0	2 517.25	124 000		
6	1 970.0	2 631.76	130 000		
6.2	2 030.0	2 714.06	135 000		
6.3	2 230.0	2 941.95	142 000		
6.4	2 300		152 600		
6.41	2 330		161 000		
6.42	2 365		165 000		
6.5	2 402		175 000		
6.6	2 510		183 000		
7	2 540		190 000		
7.1	2 600		193 000		
7.2	2 620		200 000		
7.3	2 660		215 000		
7.4	2 740		225 000		
7.5	2 790		240 000		
8	2 810		244 000		
8.2	2 900		249 000		
8.3	2 980		257 000		

Table 1 (*Continued*).

Isotope stage (upper limit)	MIS limits in core MD95-2039 depth (benthic $\delta^{18}O$) [12]	MIS limits in core MD95-2042 depth (benthic $\delta^{18}O$) [14]	Age (a) from [16,17]
8.4	3 110		266 000
8.5	3 240		289 000
8.6	3 320		299 000
9	3 340		303 000
9.1	3 380		310 000
9.2	3 470		320 000
9.3	3 520		331 000

Isotope stage ages were taken from [16,17].

netic directions. It was measured at regular intervals on paleomagnetic specimen series from cores MD95-2040 (every 50 cm) and MD95-2042 (every 20 cm), and on specimens specially collected besides U-channels in other cores. Eigenvalues K_1, K_2 and K_3 of the susceptibility tensor, as well as the declination and inclination of K_1 measured along two giant cores are presented (see supplementary Fig. 4[1]). Down to 9 m and 12 m depth, in core MD95-2040 and in core MD95-2042, respectively, a dominant lineation ($L > F$) is oriented along the vertical axis (inclination of $K_1 = 90°$). Core MD-952039 (not shown here) is also affected by this anomaly. By contrast the sediments collected with the short gravity corer present a weak foliation in the bedding plane, indicating an undisturbed primary fabric.

In intervals dominated by the vertical lineation, *apparent* sedimentation rates are twice as high as in intervals dominated by the foliation (Fig. 2). Since the transitions between the two superposed fabrics are rather abrupt and since *apparent* sedimentation rates in the top of MD95-2042 are also much higher than in cores SU81-18, MD99-2334K and MD01-2440G collected on the same site, this sedimentation rate anomaly cannot result from natural compaction (see comment no. 1[1]). Despite the fact that other studies [7–12,14,15] demonstrate the perfect stratigraphic integrity of the sequence, the paleomagnetic directions of the upper part of the sequence were taken only from short gravity cores (MD99-2334K, MD01-2440G and MD01-2441).

5. Reconstruction of paleomagnetic directions

5.1. Determination of the characteristic remanent magnetization (ChRM)

Stepwise AF demagnetization applied to pilot specimens and to U-channels shows (Fig. 3) that a soft secondary component is removed by the 5 or 10 mT AF step. Directions are then remarkably stable from 15 mT to at least up to 60 mT. The median destructive field lies between 20 and 40 mT and only 5–10% of the initial RM remains after the 60 mT treatment. The 30 mT AF step was selected to represent the directions of the stable RM (Figs. 4 and 5).

5.2. Declination and inclination variations

Several sources of errors may affect the declination profiles of the long cores: (i) a rotation of the corer about the vertical axis during its penetration in the sediment; (ii) rotation of the sediment column in sections of PVC liner during deck operations such as transport, handling and splitting. In order to present the declination profiles of the long cores, we thus performed few corrections: (i) declination values apart from section breaks were matched; (ii) long-term deviations of the declination, certainly attributed to progressive torsion of the sediment column or rotation of the corer, were corrected by linear detrending. Declination records were then rotated in order to align the mean declination value computed

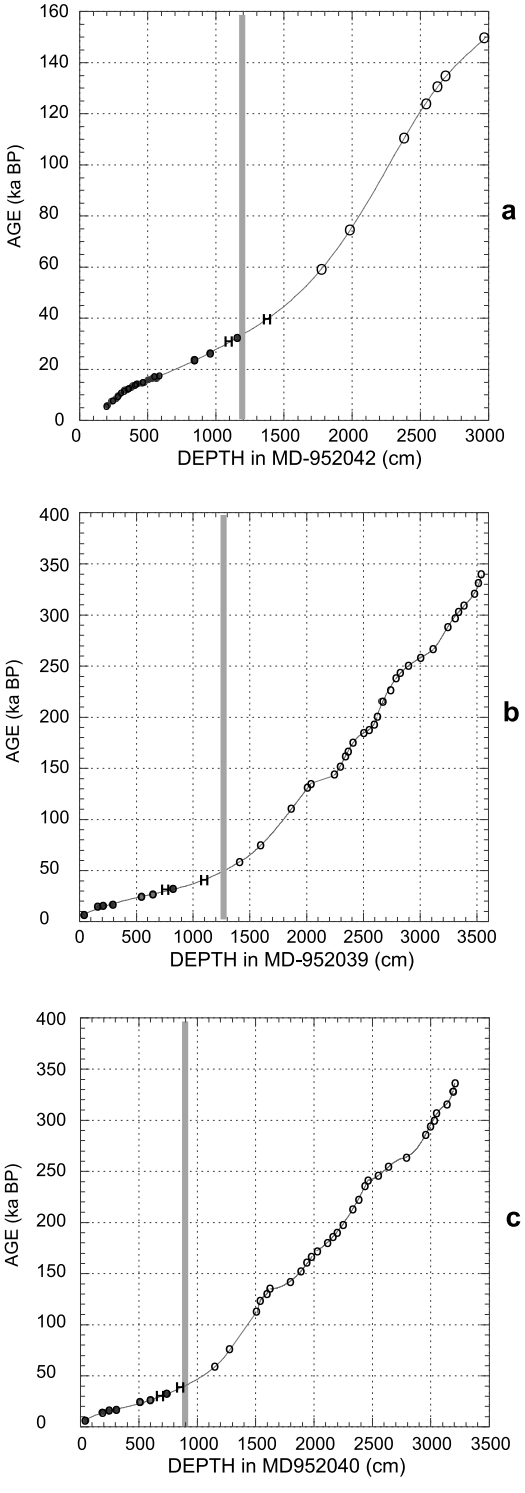

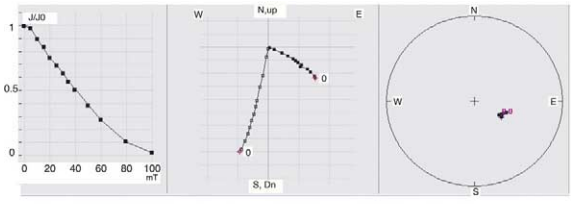

a. Core MD99-2334 K section 4 - depth 528 cm. Initial Int: 18 mA/m

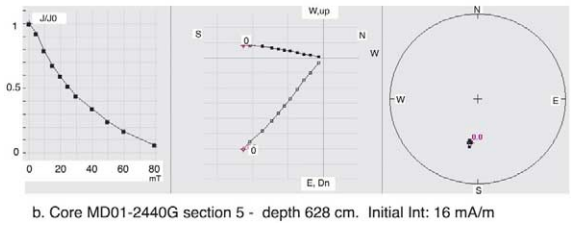

b. Core MD01-2440G section 5 - depth 628 cm. Initial Int: 16 mA/m

Fig. 3. Typical demagnetization diagrams (2G Long core datalog panel (©Bill Mills) of two layers selected in the U-channel series). (Left panels) J/J_0 decrease in AF step. (Middle panel) Orthogonal demagnetization diagrams (black and white squares concern the horizontal and vertical components respectively; 10^{-4} A/m and 10^{-5} A/m/interval of horizontal and vertical axes, respectively. (Right panels) Stereographic projection of the directions. Note that the declination is uncorrected.

along each core to the normal field average declination $D = 0°$.

Variations of the directions of the ChRM are presented in Figs. 4 and 5 after transfer from the depth scales of individual cores to the time scale. Along short cores, i.e. for the last 50 kyr (Fig. 4a), declination and inclination vary by 30° and 50°, respectively, in reasonable agreement with the rhythm and amplitude of geomagnetic paleosecular variation (PSV) recorded elsewhere (e.g. [25]). The most striking feature is a low inclination peak

←

Fig. 2. Chronological reconstruction of the sequences. Ages listed in Table 1 are plotted along the depth of each core (a: MD95-2042; b: MD95-2039; c: MD95-2040): calibrated ^{14}C ages (dots), Heinrich events 3 and 4 (H), and dated paleoclimatic markers (circles). Best fit polynomial curves were computed in successive windows to obtain age/depth functions used to transfer all data from core depth scales to the time scale. The gray vertical bands locate the transition between the anomalous (left) and normal (right) sedimentary fabrics.

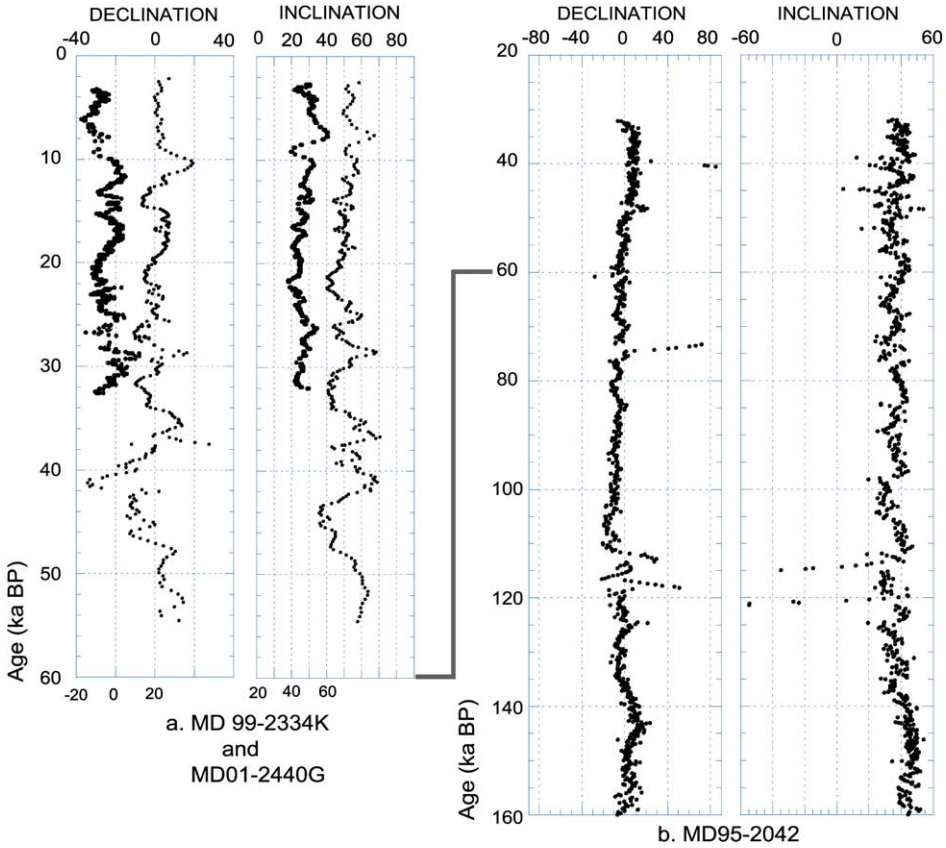

Fig. 4. Declination and inclination profiles of the stable RM along cores MD99-2334K, MD01-2440G (a) and MD95-2042 (b) on the time scale. Directions at 30 mT AF along U-channels of MD99-2334K (big dots) and MD01-2440G (small dots) (a) and on specimens of core MD95-2042 (b). Horizontal scales were shifted in order to allow inter-core comparisons (left panel) or chosen to fully express directional anomalies. Note that short core records (last 60 kyr) complete and overlap the top part of core MD95-2042 (30–160 kyr BP).

at 43 kyr BP followed by an eastward declination swing at 42 kyr BP.

In the MD95-2042 record (interval 30–160 kyr BP; Fig. 4b) and the MD95-2039 and MD95-2040 records (40–400 kyr BP; Fig. 5), regular oscillations of limited amplitude are attributable to paleosecular variation, such as those recognized in the Lac du Bouchet record for the same epoch [25,26]. This suggests that these sediments have recorded directional changes of the geomagnetic field. Anomalous paleomagnetic directions are evidenced: large declination swings occur at 40 and 74 kyr BP and between 110 and 120 kyr BP in core MD95-2042. A double westward and eastward departure to 180° is recorded between 115 and 100 kyr BP in core MD95-2039; declination swings also appear at 185, 225, 240, 295, 335 and 385 kyr BP in cores MD95-2039 and MD95-2040. Inclination departures often occur near the time of declination swings: in core MD95-2042 (Fig. 4b), the inclination reach −55° at 122 kyr BP and −40° at 115 kyr BP. In core MD95-2040 (specimen series) (Fig. 5b) the inclination reaches −45° at 188 kyr BP and −25° at 290 kyr BP. These negative inclination features are limited to low inclination (20°) peaks along the U-channel series, which are probably affected by the convolution imposed by continuous measurements.

Such directional anomalies evidence large but transient departures from the paleosecular varia-

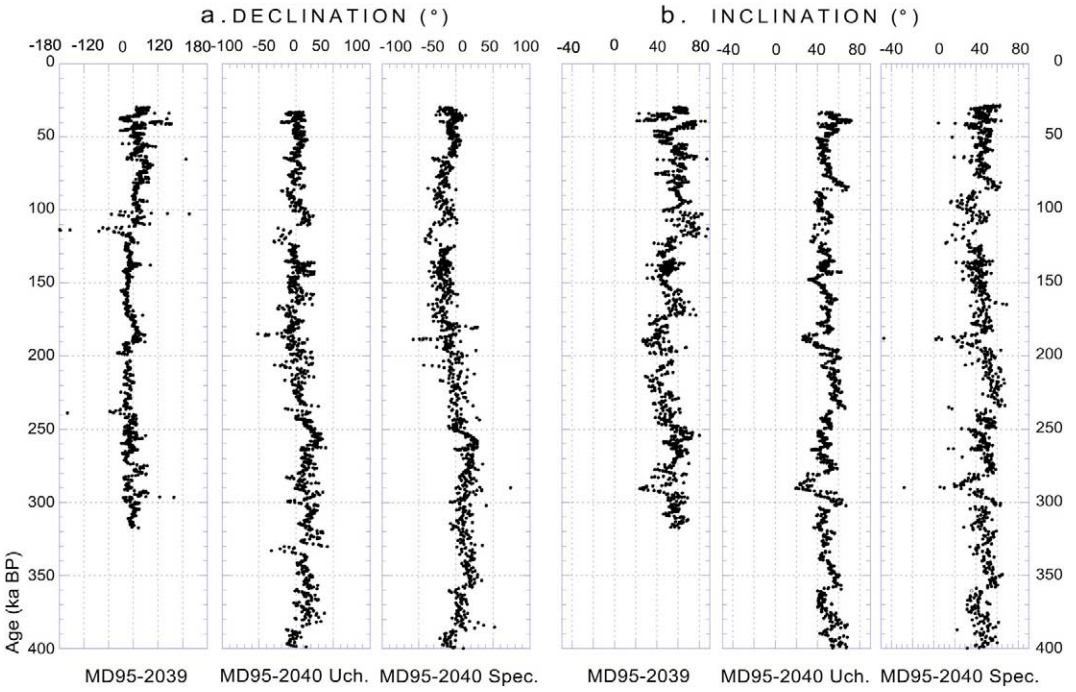

Fig. 5. Declination (a) and inclination (b) profiles on the time scale for the interval 40–400 kyr BP. U-channels and specimens series collected along cores MD95-2039 and MD95-2040. For each case, horizontal scales were selected in order to express directional anomalies. Results obtained on U-channels and specimens along core MD95-2040 are compatible despite a relatively larger noise on the specimen series; the largest amplitude of the signals expresses excursional directions.

tion regime, assignable to paleomagnetic excursions. Therefore, the occurrence of excursions is supported by both declination swings and inclination anomalies at 115–125 kyr BP, at 185–190 kyr BP and at 290 kyr BP. Declination swings or inclination anomalies may document other excursions at 42, 75, 95, 240, 335 and 385 kyr BP.

5.3. Stacking inclination records

Unfortunately, the declination and inclination records are too noisy to allow the construction of a type record. An inclination stack will however provide a useful reference to evidence paleomagnetic excursions during the last 400 kyr. In order to align the different inclination records, we had to: (i) account for latitudinal differences between the two studied areas and (ii) correct inclination errors (see comment no. 2[1] and Table 2[1]). We thus computed $\delta I = I - I_{bar}$, i.e. the difference between individual inclinations and the mean inclination computed along each core (excluding excursional data). All corrected inclination records were then merged.

6. Normalization of NRM intensities

6.1. Principles

RPIs were evaluated by normalization of the NRM using the rock magnetic parameters susceptibility χ, IRM and ARM, as suggested by the review paper of Tauxe [27]. The most significant parameters and their ratio are compared with $\delta^{18}O$ and carbonate content records from same cores.

Susceptibility χ and IRM profiles (Figs. 6b and 7b) are affected by abrupt increases due to IRD fraction, although these layers are relatively thin

and the IRD fraction diluted with the sediment matrix. Furthermore, a long-term evolution of their amplitude over the successive climatic cycles is observed (e.g. Fig. 7b). Therefore, even if χ and IRM values carried by IRD layers can be removed from the data sets, short-, medium- and long-term trends could be responsible for major biases of the NRM normalization.

The ARM here expressed as anhysteretic susceptibility (χ_{ARM}) (Figs. 6c and 7c) is carried by SD, pSD and small MD grains of Ti-magnetite, i.e. the fraction concerned in the depositional remanent magnetization (DRM). Significant relationships between χ_{ARM}, χ_{ARM}/χ and $CaCO_3$ % and $\delta^{18}O$ (Figs. 6a,c,d and 7a,c,d) demonstrate that concentration and grain size of the NRM carriers are in phase opposition with the carbonate content variations (see also [9,10]). This suggests that if magnetic interactions [28] and maghemitization [29] are negligible, the ARM should constitute an appropriate parameter to normalize NRM intensity variations (Figs. 6e and 7e) due to variations of concentration of NRM carriers. The variations of the NRM/ARM demagnetized at 30 mT demagnetization step are presented in Figs. 6f and 7f.

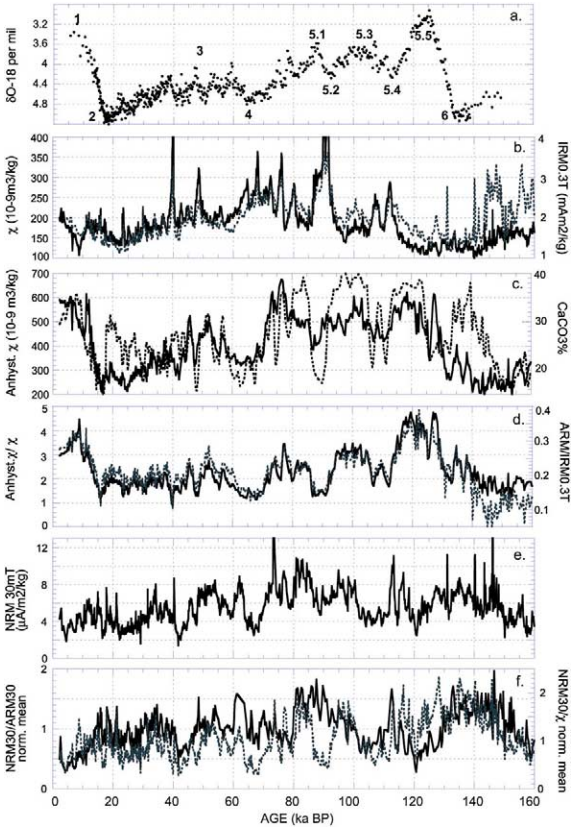

Fig. 6. Isotopic data [14,15], carbonate data [8] and rock magnetic parameters along core MD95-2042 plotted on the time scale (last 160 kyr). (a) $\delta^{18}O$ profile. (b) χ (full line) and SIRM (gray broken line). (c) χ_{ARM} (full line) and $CaCO_3$ (gray broken line). (d) χ_{ARM}/χ (full line) and $ARM/IRM_{0.3T}$ (gray broken line). (e) NRM. (f) NRM/ARM (full line) and NRM/χ (gray broken line) after normalization to their respective mean values.

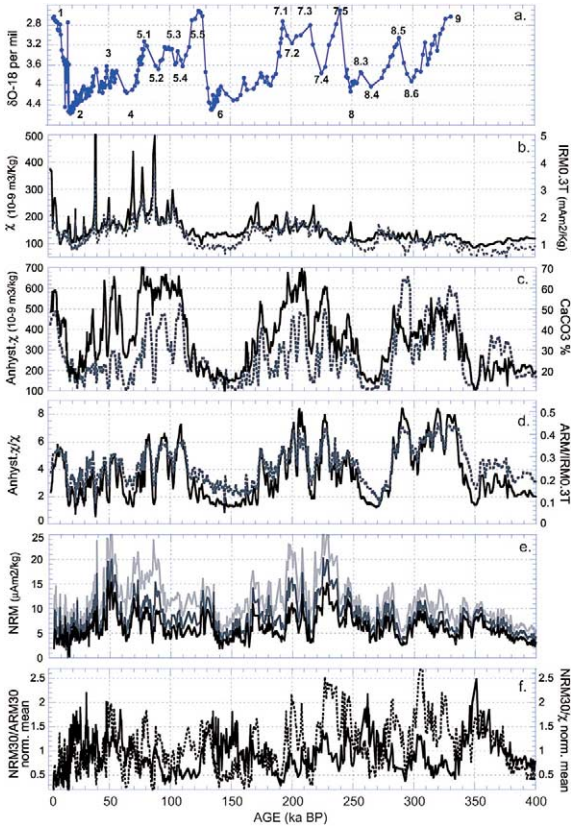

Fig. 7. Isotopic data [12] and carbonate data [8,12] compared with rock magnetic parameters along core MD95-2040, plotted on the time scale (last 400 kyr). (a) $\delta^{18}O$ profile of MD95-2039. (b) χ (full line) and SIRM (gray broken line). (c) χ_{ARM} (full line) and $CaCO_3$ (gray broken line). (d) χ_{ARM}/χ (full line) and $ARM/IRM_{0.3T}$ (gray broken line). (e) Uncleaned NRM (light gray) and AF 20 (gray) and 30 mT (black). (f) NRM/ARM (full line) and NRM/χ (gray broken line) after normalization to their respective mean values.

6.2. The normalization method and its efficiency

For discrete specimens, the NRM demagnetized at 30 mT was normalized by the ARM at 30 mT. For U-channels, NRM and ARM were demagnetized at 10, 20, 30, 40 and 60 mT and NRM/ARM ratios were computed for each step. Because NRM have lower hardness spectra than ARM, the use of increasing AF field values leads to the increase of both the NRM_i/ARM_i ratios and the amplitude of variation. For each individual layer, average values of the NRM_i/ARM_i ratio and their standard deviation were computed. This method constitutes a simple alternative to the 'pseudo-Thellier' methods developed by Tauxe et al. [30] and by Valet and Meynadier [31]. All NRM/ARM ratios obtained along a core were normalized by the mean NRM/ARM ratio computed along that core.

The efficiency of NRM normalizations can be tested by evaluating the correlation between normalized intensities and normalizing parameters (ARM, IRM or χ) (e.g. [26]) or, as recommended [32], by measuring their degree of coherence (correlation in the frequency domain). Along core MD95-2040, the NRM/ARM and the susceptibility profiles exhibit common periods near 22 and 15 kyr (Fig. 8a,b) but have no significant coherence (Fig. 8d). A weak inverse correlation between NRM/ARM and ARM or ARM/χ ($r=-0.4$ and -0.5, respectively) is confirmed by similar power spectra (Fig. 8b,c) mostly near Milankovitch frequencies, and by significant coherences (Fig. 8e). These observations may suggest that the long-term variability of the NRM/ARM curve is influenced by concentration, grain size, and/or by the degree of maghemitization.

The relationship between the NRM/ARM profile and paleoclimatic variations is suggested by a relationship with $CaCO_3$ % ($r=0.46$) and supported by a significant correlation with the $\delta^{18}O$ record ($r=0.62$). This correlation is stronger ($r=0.78$) when NRM/ARM peaks are shifted towards the past by $\sim$18 kyr. This observation casts doubt about the reliability of our normalized intensity record despite the remarkable agreement between our records of the last 60 kyr (Fig. 9a–d) and other RPI reference curves [5,6].

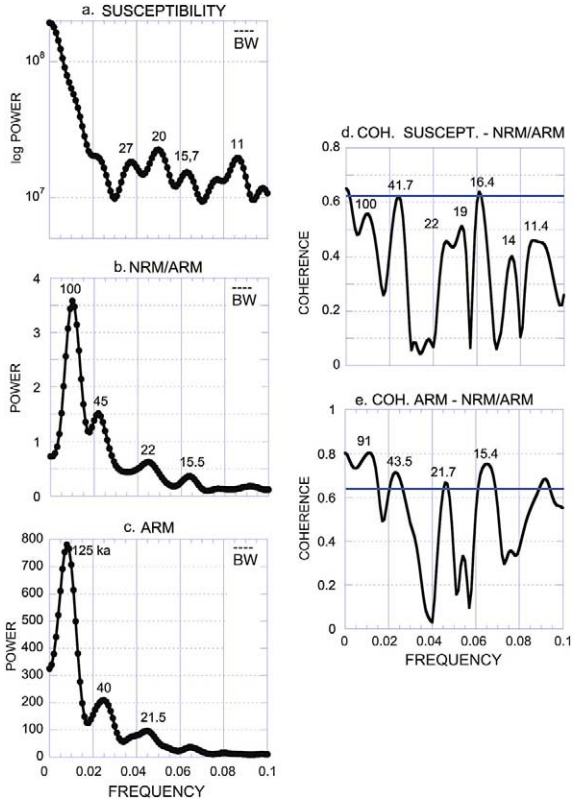

Fig. 8. Power spectra (power as a function of frequency in kyr^{-1}) computed along data sets of core MD95-2040 [Blackman–Tukey (BT) method with a Bartlett window, bandwidth = 0.007; the confidence interval at 95% $\Delta P/P$ is comprised between 0.64 and 1.78]. (a) Susceptibility (χ). (b) NRM/ARM. (c) ARM. (d,e) Cross-coherence spectra between: (d) χ and NRM/ARM and (e) ARM and NRM/ARM. The thick horizontal line is the 95% confidence interval for zero coherence.

7. Construction and smoothing of the Portuguese margin RPI record

7.1. Analytical procedures

Given the precise location and identification of susceptibility peaks, the transfer on the time scale based on inter-core age transfer (see Section 2) introduces negligible stratigraphic errors. However, at different localities magnetic grains are aligned under different local conditions; this imposes slightly different lock-in functions of the DRM and pDRM. Therefore, paleomagnetic sig-

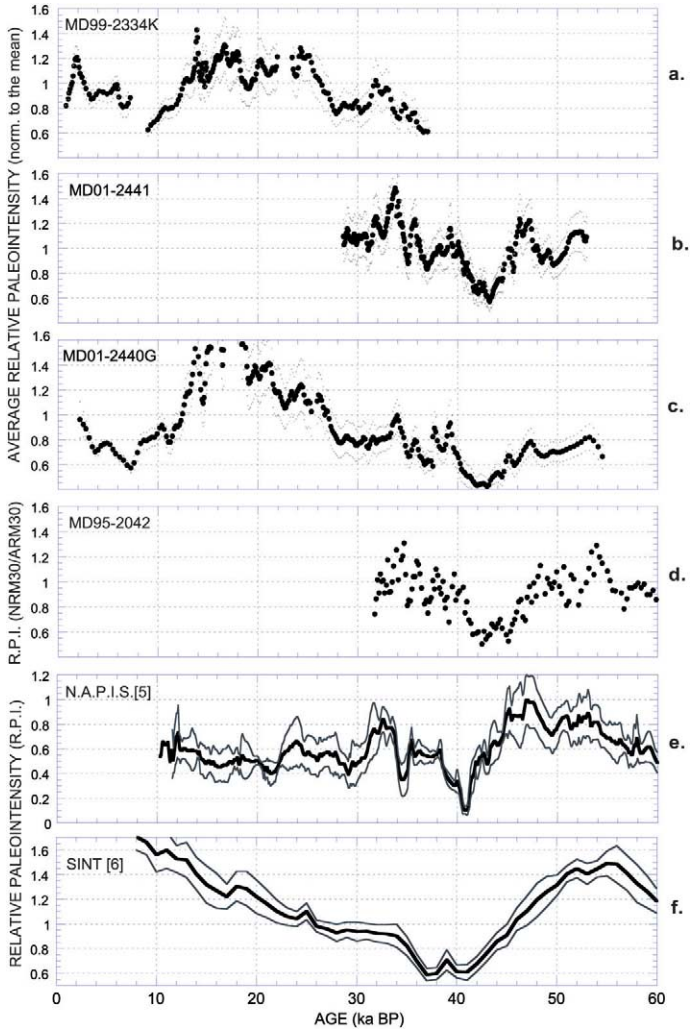

Fig. 9. Average RPI profiles for the interval 0–60 ka obtained along cores MD99-2334K, MD01-2441, MD01-2440G, MD95-2042 (top) (average ± 1σ computed from retained AF steps) and comparison with records of the reference curves NAPIS [5] and SINT 200 [6].

natures recorded in different cores are not perfectly aligned (Figs. 9 and 10). However, the process of peak realignment is rather subjective. All RPI profiles available (Figs. 9a–d and 10a–d) were stacked and a smoothing procedure was applied on the stacked record (Fig. 10e). We used a robust procedure of locally weighted regression (LOWESS or LOESS [33]). Let y_i, $i=1,...,n$ be a collection of n measurements of a response variable y and x_i, $i=1,...,n$ a corresponding predictor vector. Suppose that the data are related by $y_i=f(x_i)+\varepsilon_i$ where the ε_i are normal (see below) independent variables with zero mean and variance σ^2, and $f(x)$ is the value of a function at x. The local regression assumes that near $x=x_0$, the regression function $f(x)$ can be approximated by the value of a function $\hat{f}(x)$ in some specified parametric class.

In the present case, $\hat{f}(x)$ was considered as a sequence of polynomials of degree 1. The local approximation was obtained by fitting a linear regression function to the data points within a given neighborhood of the point x_0. In our case, the weighted least squares method was used to fit

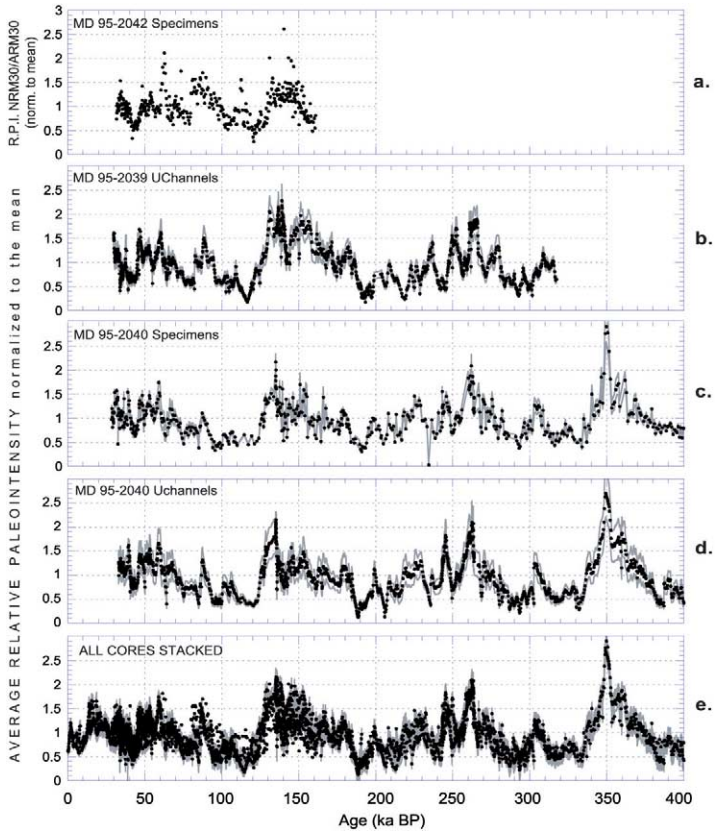

Fig. 10. Average RPI profiles obtained for the 0–400 kyr BP time interval. (a) Core MD95-2042 (specimens). (b) MD95-2039 (U-channels). (c,d) MD95-2040 (specimens and U-channels, respectively). (e) Stack of all NRM/ARM profiles of Figs. 9 and 10.

a linear function of the predictor at the center of neighborhoods. Each neighbor point was weighted according to a weight polynomial function. The smoothness of the fit, i.e. the influence of the weight function onto the neighbor points, was controlled by a smoothing parameter estimated by a general cross-validation procedure.

A quantile–quantile plot (Fig. 11a) and a two-sided Kolmogorov–Smirnov test for goodness of fit ($P \approx 0.27$) justify the assumption of a Gaussian distribution of the noise around the RPI data presented in Fig. 10e. We thus computed a 99% pointwise confidence interval presented along the smoothed RPI curve (Fig. 11b).

7.2. Relation with paleomagnetic directions

Smoothed normalized intensities fluctuate between 20 and 250% of the average value. Low RPI episodes are recorded at ~10, 40, 75, 95–125, 190, 205–215, 240, 255, 285–295, 315–330 and 385–400 kyr BP; maximum RPI values are recorded at 20, 60, 85, 135, 150, 230, 245, 260 and 350 kyr BP. Due to the large noise introduced by the stacking, large amplitude deviations accurately documented in individual inclination records would be completely erased by any smoothing procedure. Considering a possible attenuation of the paleomagnetic variations by DRM and pDRM processes, the extreme deviations of the directions (Figs. 4 and 5) probably represent minimum estimates of the actual geomagnetic deviations. The comparison of the smoothed RPI record (Fig. 11b) with the raw inclination stack (Fig. 11c), with reference to major declination swings, demonstrates that each significant deviation from the axial dipole direction occurs within a low RPI interval.

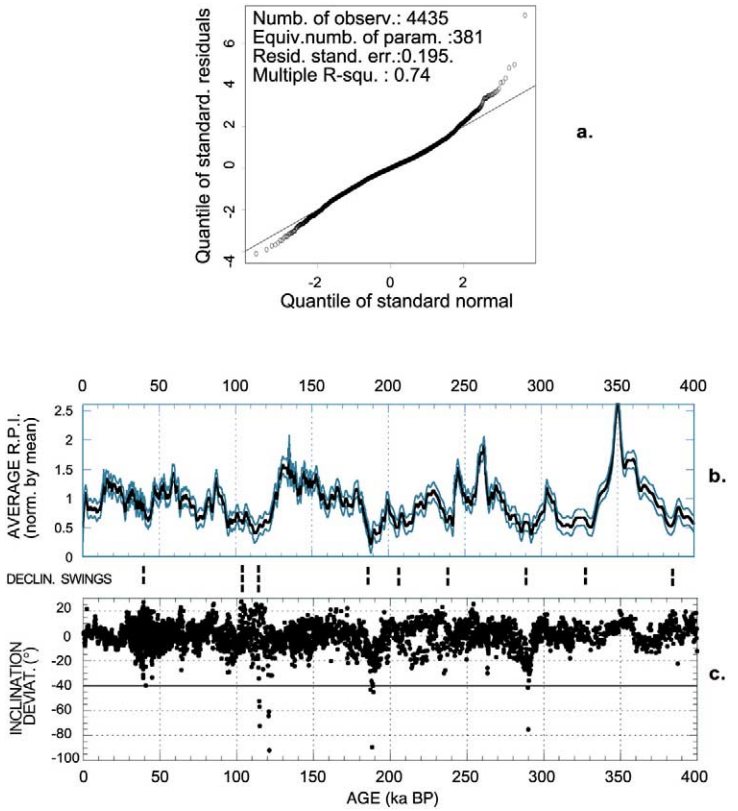

Fig. 11. (a) Gaussian quantile plot of standardized residuals. (b) Smoothed RPI record (black line) estimated by a regression method [33], and 99% pointwise confidence interval (gray lines). (c) Stacked record of δI values. The black horizontal line shows the limit between PSV and excursions. Dotted bars indicate the ages of significant declination swings associated with excursions (three dots indicate fully reversed declinations).

8. Normalized intensity record as geomagnetic paleointensity proxies?

As introduced in Section 6, normalized intensities can be biased by concentration, grain size, oxidation degree of the magnetic carriers, etc. Kok and Tauxe [34] also introduced the possible contribution of long-term viscous remanent magnetization (VRM) linked with lithological changes presumably of diagenetic origin. Some of their results indicated that sediments deposited during warm periods carry relatively higher long-term VRM. The detection of such current biases is not straightforward. Reconstructing a NRM/ARM profile from a synthetic NRM record of field intensity affected by variable responses to climatically driven ARM variations, Valet [35] showed that spectral analyses are not efficient enough to reveal the coherence between NRM/ARM and ARM records; wavelet analysis is required. These results lead to rather pessimistic conclusions about the efficiency and reliability of NRM normalization. However, recently Tauxe and Love [36] compared the SINT 800 [6] with the near-seafloor magnetic anomaly record of the southern East Pacific Rise [37] and noticed a remarkable compatibility between tiny wiggles and RPI highs and lows.

8.1. *Comparison of Holocene RPI data with the archeomagnetic record*

Because the uppermost sediments are generally affected by coring deformation or by oxidation, the

data of the last 10 kyr are often absent from RPI records. In this study, the use of light and short corers provided two well-preserved core tops containing oxidized carbonate ooze used to establish a Holocene RPI record. However, RPI data of the 10–20 kyr BP interval are recovered from unoxidized late glacial and glacial clayey muds.

The average RPI record obtained from the two available cores has been compared with the absolute VADM (virtual axial dipole moment) record compiled by McElhinny and Senanayake [38] recently completed by Yang et al. [39] (see supplementary Fig. 5[1]). For the last 10 kyr, the agreement is satisfying: starting with medium values at 10 kyr BP, VADM and RPI decrease down to a minimum at ~7 kyr BP; then they progressively

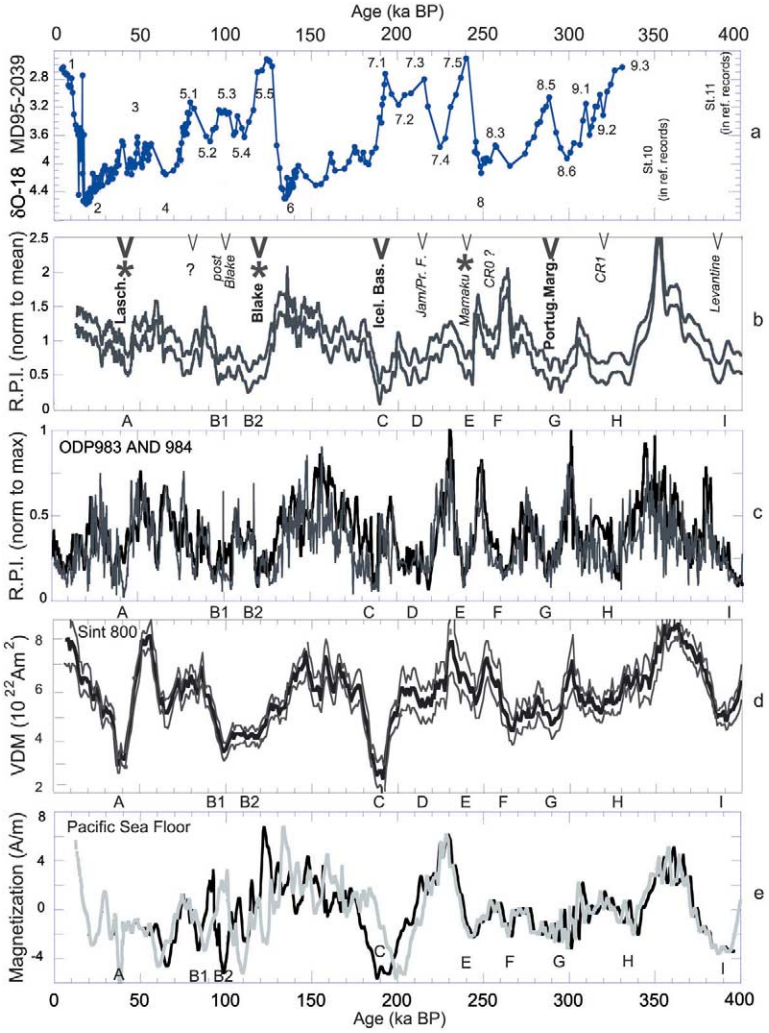

Fig. 12. Comparison of different paleointensity proxy records (last 400 kyr) with reference to $\delta^{18}O$ (a) of core MD95-2039 [12]. (b) The smoothed Portuguese stack (99% confidence interval) is compared with (c) ODP sites 983 and 984 [41] and (d) SINT 800 (VDM values in 10^{22} Am^2) [6]. (e) Reconstructed remanent magnetization of the East Pacific seafloor record [37] on its original time scale (gray line) and on a modified time scale (black line). Identification labels (A–I) at their respective age in each record underline the correlation between the different records. In panel b, excursions are indicated by big 'V' and non-excursional deviations by small 'v'. Excursions recorded in lava flows are distinguished by asterisks. A relationship between RPI lows and interglacial or interstadial stages is evidenced (see also Table 2).

increase, with a marked step at 4 kyr BP, up to maximum values at 2.5–3 kyr BP. However, from 14 to 10 kyr BP, the large and regular decrease of RPI data is in contradiction with the absolute VDM (virtual dipole moment) data recently compiled [40]. This RPI trend is recorded in the transition from non-oxidized to oxidized sediments and must be considered with suspicion.

8.2. Comparison of the Portuguese RPI records with other RPI reference records

The RPI stack is presented along the $\delta^{18}O$ record of the same sequence (Fig. 12a,b). It is compared with the RPI records from North Atlantic ODP sites 983 and 984 [41] and with the 0–400 kyr BP interval of SINT 800 [5] (Fig. 12c,d). Long-term oscillations present similar wavelengths but have rather different amplitudes. For example, the large amplitude peak located between 320 and 380 kyr BP in our record is much larger than in the SINT curve. Between 130 and 260 kyr BP, our record presents relatively smaller amplitudes than other records. For the last 120 kyr, the amplitudes are reduced (40–140%); namely, a narrow drop at 42 kyr BP is attenuated in comparison with other records. Major phase shifts can be explained by inconsistencies in the determination and/or dating of $\delta^{18}O$ stage boundaries. The common structure of all RPI records is marked by a succession of low RPI intervals, labelled A–I. The seafloor magnetization record of the southern East Pacific Rise [37] (Fig. 12e) also documents major low intervals. Its original chronology (gray curve) can be slightly modified (black curve) to match the chronological positions of the A–I intervals in the sedimentary RPI records. Such adjustment is compatible with the chronological errors imposed by the assumption [37] of constant expansion rates of the East Pacific Rise since the Brunhes–Matuyama boundary.

9. Paleointensity lows, excursions and events in the last 400 kyr

In this section, we analyze the synchronicity of RPI lows with paleomagnetic excursions or events. Excursions are defined by paleomagnetic vector deviations of at least 40° from the geocentric axial dipole field direction. Short events are defined by stabilization in fully reversed directions for few millennia. Therefore, except the fully reversed Blake *event* (e.g. [42]), paleomagnetic anomalies reported for the Brunhes epoch rather follow the definition of 'excursions'. Fig. 11 evidences that four low RPI intervals coincide with inclination and declination anomalies (see also Figs. 4 and 5). Other RPI lows do not correspond to excursional directions but they occur at the ages of dated excursions.

- **Interval A** centered at 42 kyr BP is correlated with the Laschamp excursion [43]. The directional patterns (see Section 5.2 and Fig. 4a) mimics those attributed to the Laschamp excursion at Lac du Bouchet and Lac St Front [44,45] and those attributed to the Mono Lake excursion at Mono Lake [46]. This similarity indicates that both excursions have identical paleomagnetic signatures in different sites. It may alternatively suggest, as claimed by Kent et al. [47], that the Mono Lake excursion is a record of the Laschamp, although recent findings of two independent excursions at Summer Lake (Oregon, USA) (R. Negrini, personal communication) support the occurrence of two independent excursions.
- At 75 kyr BP, a slight RPI low, also located in lake [26,48] and marine [5,6] records, may be in relation with an excursion observed in the Norwegian-Greenland sea cores [4].
- **Interval B** (95–125 kyr BP) is divided into subintervals. The youngest one (B1) does not contain excursional directions, but occurs at ~95 kyr BP, the age of an excursion revealed in the Lac du Bouchet record [25] and called here 'post-Blake' excursion. The oldest one (B2) contains two large amplitude inclination anomalies (at 115 and 122 kyr BP), accompanied by two large declination swings. It represents the Blake event frequently reported from marine or cave sediment studies (e.g. [42,49]), and recently dated by thermoluminescence between 114 and 120 kyr BP in a Chinese loess soil sequence [50].

- **Interval C** (185–198 kyr BP) is characterized by extremely weak RPI values. A deviation of 90° from the geocentric axial dipole inclination and a large amplitude declination swing reveal an excursion at the exact age of the 'Icelandic basin' excursion, a transient reversal defined at ODP sites 983 and 984 [41] and recognized in the Lake Baikal sequence [51].
- **Interval D** (205–215 kyr BP) occurs in the age range of the Jamaica and Pringle Falls excursions: the Pringle Falls tephra was dated by $^{40}Ar/^{39}Ar$ at 218 ± 10 kyr BP [52].
- **Interval E** occurs at 240 kyr BP. It is a better candidate than interval D for a correlation with the Mamaku excursion, dated at 230 ± 12 kyr BP by $^{40}Ar/^{39}Ar$ dating on an ignimbrite [53], and formerly correlated with the Pringle Falls excursion [54].
- **Interval F** is a slight but significant RPI drop occurring at ~255 kyr BP, i.e. near the age of the Calabrian Ridge 0 excursion in the Mediterranean core KC01B [55].
- **Interval G**, centered at 290 kyr BP, is associated with a large amplitude declination swing followed by an inclination anomaly. Two excursions formerly defined in this time interval are not appropriate candidates: (i) the Levantine excursion was actually re-located in older sediments [55] and (ii) the reliability of the Biwa II excursion in Lake Biwa cores [56] was questioned. We propose to name this excursion 'Portuguese margin'. Its coincidence with MIS 8.5 constrains an age around 290 kyr BP: the Amargier interstadial, equivalent of MIS 8.5, was dated by $^{39}Ar/^{40}Ar$ at 275 ± 5 kyr BP on tephra layers of the Lac du Bouchet and Praclaux sequences [26,57].
- **Interval H** (315–330 kyr BP) occurs at the time of the Calabrian Ridge 1 excursion described in core KC01B [55].
- **Interval I** (390 kyr BP), documented in ODP sites 983 and 984, is rather attenuated in the SINT curve. It occurs at the age of the Levantine excursion [55].

10. Relationships with isotope stages and Milankovitch periodicities

The presence of orbital periodicities in paleomagnetic records has been strongly debated. Spectral analyses of separate windows along the SINT 800 record failed to reveal dominant periods [6]. Over the last 5.3 Myr (resp. 0.78 Myr), reversals

Table 2
Major RPI features and related excursions are listed with the corresponding marine isotope stages (bold characters distinguish excursions recorded as directional anomalies in the studied cores)

RPI interval	Related excursion or short event	Age (kyr BP)	Marine isotope stage
Low A	**Laschamp**	42	interstadial MIS 3 (ice cores i.s. 10)
Unlabelled Low	**Norwegian-Greenland**	75	interstadial MIS 5.1
Low B1	Post-Blake	95	interstadial MIS 5.2
and B2	**Blake**	115–122	interglacial MIS 5.3
High B/C		*132*	*glacial MIS 6*
Low C	**Icelandic basin**	190	interglacial MIS 7.1
Low D	Jamaica-Pringle Falls	210	interglacial MIS 7.3
Low E	Mamaku	240	interglacial MIS 7.5
Low F	Calabrian Ridge 0	255	glacial MIS 8 (interst. 8.3)
High F/G		*265*	*glacial MIS 8*
Low G	**Portuguese margin**	290	interstadial MIS 8.5
High G/H		*305*	*glacial MIS 8.6*
Low H	Calabrian Ridge 1	315–335	interglacial MIS 9 (9.1 to 9.3) transition to MIS 8.6
High H/I		*355*	*glacial MIS 10* [16,61]
Low I	Levantine	385–400	Interglacial MIS 11 [16,61]

Note the rather systematic correspondence between (1) RPI low, (2) excursions and (3) interglacial or interstadial stages.

(resp. excursions) do not present a ''discernible tendency to occur at consistent amplitude or phase of obliquity nor excentricity'' [58]. On the other hand, in the ODP 983 record, periods of 100, 42, 23 and 19 kyr appear to be independent of lithologic effects [41]. Wavelet analyses of a 700 kyr RPI record from the Pacific Ocean [59] revealed a 100 kyr period, as well as a phase relationship between RPI and $\delta^{18}O$ with a lag of 18 kyr of the RPI signal versus interglacials. Orbital periods were also found in inclination and RPI records for the last 2.25 Myr [60].

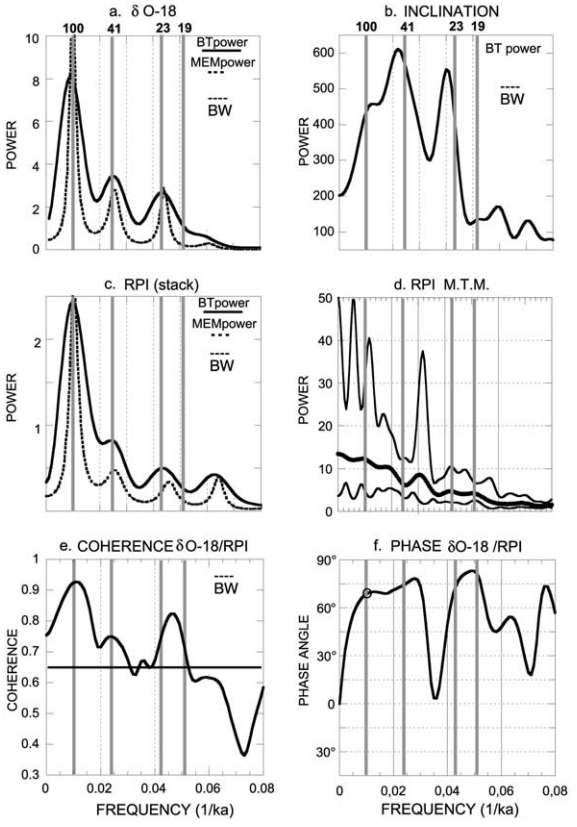

Fig. 13. Power spectra computed with the Analyseries program [62] using the Blackman–Tukey (BT) (confidence interval at 95% $\Delta P/P$ is comprised between 0.64 and 1.78) and the maximum entropy method (MEM). (a) $\delta^{18}O$. (b) RPI. (c) Inclination. (d) Power spectra (thick line) and 95% confidence intervals obtained using the Multitaper method. (e) Cross-coherence and (f) phase diagram of $\delta^{18}O$ and RPI. The thick horizontal line is the 95% confidence limit for zero coherence; the circle indicates the lag ($\sim 68° = 18$ kyr) between RPI and $\delta^{18}O$ for the 100 kyr period.

The comparison of paleointensity records with the benthic $\delta^{18}O$ record of core MD95-2039 (and $\delta^{18}O$ key records [16,61]) evidences that RPI lows and accompanying excursions occurred during interglacial or interstadial stages, or at the boundary with the following glacial (Fig. 12a,b and Table 2). This relationship was further evidenced using spectral and cross-coherence analyses [62]. The methods used are: (i) the maximum entropy method and (ii) the Blackman–Tukey method (Bartlett window; bandwidth = 0.007, confidence interval = 95%). The $\delta^{18}O$ and the RPI records (and to a lesser extent the inclination record) present a major common period at 100 kyr and minor periods at 41 kyr and 23 kyr (Fig. 13a–c). The Multitaper method (six windows, bandwidth = 0.004) suggested by Tauxe [27] shows a reduced 100 kyr period and an emerging 33 kyr period (Fig. 13d) but a complex wavelet analysis (G. Saracco, personal communication) confirms the dominance of the 100 kyr period (article in preparation). A significant coherence between $\delta^{18}O$ and RPI variations is revealed (Fig. 13e,f), with a phase shift of 60°, equivalent to a duration of $\sim$18 kyr, already evidenced [59].

11. Conclusion

In agreement with other relative geomagnetic moment proxy records [6,41,37], the Portuguese margin paleomagnetic record documents recurrent geomagnetic moment drops in the last 400 kyr. Low RPI intervals were labeled by letters A–I. Three directional anomalies dated at 42 kyr BP, at 115–122 kyr BP and at 190 kyr BP, occurring in RPI lows A, B and C, are correlated with the Laschamp excursion, the Blake event and the Icelandic basin excursion, respectively. The RPI low labeled G, dated at 290 kyr BP, contains another excursion named here the 'Portuguese margin' excursion. Four non-excursional RPI lows occur at, or near, the ages of the Jamaica/Pringle Falls, Mamaku, Calabrian Ridge 1 and Levantine excursions.

Spectral analyses of the RPI record reveal a dominant periodicity at 100 kyr, already reported by other studies (e.g. [41,59,60]). The RPI and

$\delta^{18}O$ records also present a phase shift of 18 kyr: RPI lows often coincide with the end of interglacial or interstadial stages.

The geomagnetic moment loss (−30%) over the last two millennia deduced from archeomagnetic results (e.g. [38,39]) might foreshadow the next excursion for the end of our present interglacial, even though this loss started 2200 years ago from an exceptionally high geomagnetic moment value.

The construction of the authigenic $^{10}Be/^{9}Be$ record from the same sedimentary sequence [1] supports the validity of the Portuguese margin RPI record.

Acknowledgements

Cores were collected by the technical crew of the R.V. *Marion Dufresne* under the direction of Y. Balut. IMAGES campaigns were funded by 'I.F.T.R.P.' (presently I.P.R.E.V. for Institut de Recherche Paul-Emile Victor). We thank Yves Lancelot and J.L. Turon, Chief Scientists of MD-101 (1995) and MD-123 (2001), respectively, as well as F. Grousset and S. Berné for assisting N.T. during MD-114 (IMAGES 5 leg 5, 1999). Nick J. Shackleton and J. Schönfeld provided $\delta^{18}O$ data of cores MD95-2042 and MD95-2039. Jim Channel kindly provided data of ODP sites 983 and 984 and J. Gee kindly provided data of the near-seafloor anomaly record. Fruitful discussions with E. Bard, D.-L. Bourlès and P. Rochette are acknowledged. We thank Lisa Tauxe for careful and detailed reviews that enabled a considerable improvement of the manuscript. Thanks are due to Christine Paillès and Cathy Faidix for the corrections of the English writing. This study was partly funded by the INSU program 'Intérieur de la Terre' to N.T. and D. Bourlès from 2000 to 2003.***[BOYLE]***

References

[1] J. Carcaillet, D.L. Bourlès, N. Thouveny, M. Arnold, A high resolution $^{10}Be/^{9}Be$ record of geomagnetic moment variations over the last 300 ka from sedimentary cores of the Portuguese Margin, Earth Planet. Sci. Lett. doi: 10.1016/S0012-821X(03)00702-7, this issue.

[2] D.E. Champion, M.A. Lanphere, M.A. Kuntz, Evidence for a new geomagnetic reversal from lava flows in Idaho: Discussion of short polarity reversals in the Brunhes and late Matuyama polarity chrons, J. Geophys. Res. 93 (1988) 11667–11680.

[3] N.D. Opdyke, J.E.T. Channel, Magnetic Stratigraphy. International Geophysics Series. Academic Press, London, 1996, pp. 242–249.

[4] N.R. Nowaczyk, T.W. Frederichs, Geomagnetic events and relative paleointensity variations during the past 300 ka recorded in Kolbeinsey ridge sediments, Iceland sea: indication for a strongly variable geomagnetic field, Int. J. Earth Sci. 88 (1999) 116–131.

[5] C. Laj, C. Kissel, A. Mazaud, J.E.T. Channel, J. Beer, North Atlantic paleointensity stack since 75 ka (NAPIS-75) and the duration of the Laschamp event, Phil. Trans. R. Soc London 358 (2000) 1009–1025.

[6] Y. Guyodo, J.-P. Valet, Global changes in intensity of the Earth's magnetic field during the past 800 kyr, Nature 399 (1999) 249–252.

[7] O. Cayre, Y. Lancelot, E. Vincent, M.A. Hall, Paleoceanographic reconstructions from planktonic foraminifera off the Iberian Margin: temperature, salinity and Heinrich events, Paleoceanography 14 (1999) 384–396.

[8] D. Pailler, E. Bard, High frequency paleoceanographic changes during the past 140,000 years recorded by the organic matter in sediments off the Iberian margin, Palaeogeogr. Palaeoclimatol. Palaeoecol. 181 (2002) 431–452.

[9] N. Thouveny, E. Moreno, D. Delanghe, L. Candon, Y. Lancelot, N.J. Shackleton, Rock-magnetic detection of distal ice rafted debris: clue for the identification of Heinrich layers on the Portuguese margin, Earth Planet. Sci. Lett. 180 (2000) 61–75.

[10] E. Moreno, N. Thouveny, D. Delanghe, I.N. McCave, N.J. Shackleton, Climatic and oceanographic changes in the Northeast Atlantic reflected by magnetic properties of sediments deposited on the Portuguese margin during the last 340 ka BP, Earth Planet. Sci. Lett. 202 (2002) 465–480.

[11] E. Bard, M. Arnold, P. Maurice, J. Duprat, J. Moyes, J. Duplessy, Retreat velocity of the North Atlantic polar front during the last deglaciation determinated by 14C accelerator mass spectrometry, Nature 328 (1987) 791–794.

[12] J. Thomson, S. Nixon, C.P. Summerhayes, J. Schonfeld, R. Zahn, P. Grootes, Implications for sedimentation changes on the Iberian margin over the last two glacial/interglacial transitions from $(^{230}Th_{excess})_0$ systematics, Earth Planet. Sci. Lett. 165 (1999) 255–270.

[13] E. Bard, Geochemical and geophysical implications of the radiocarbon calibration, Geochim. Cosmochim. Acta 62 (1998) 2025–2038.

[14] N.J. Shackleton, M. Hall, E. Vincent, Phase relationship between millennial scale events 64,000–24,000 years ago, Paleoceanography 15 (2000) 565–569.

[15] N.J. Shackleton, M. Chapman, M.F. Sanchez-Goni, D.

Pailler, Y. Lancelot, The classic marine isotope substage 5e, Quat. Res. 58 (2002) 14–16.
[16] D.G. Martinson, N.G. Pisias, J.D. Hays, J. Imbrie, T.C. Moore, N.J. Shackleton, Age dating and the orbital theory of the ice ages: development of a high-resolution 0 to 300,000 year chronostratigraphy, Quat. Res. 27 (1987) 1–29.
[17] J. Imbrie, J.D. Hays, D.G. Martinson, A. McIntyre, A.C. Mix, J.J. Morley, N.G. Pisias, W.L. Prell, N. Shackleton, The orbital theory of Pleistocene climate: support from a revised chronology of the marine $\delta^{18}O$ record, in: A. Berger et al. (Eds.), Milankovitch and Climate, Part I, Reidel, Boston, MA, 1984, pp. 269–305.
[18] L. De Abreu, N.J. Shackleton, J. Schönfeld, M. Hall, M. Chapman, Millenial scale oceanic climate variability off the western Iberian margin during the last two glacial periods, Mar. Geol. 196 (2003) 1–20.
[19] P. Rochette, F. Vadeboin, L. Clochard, Rock magnetic application of Halbach cylinders, Phys. Earth Planet. Inter. 4026 (2001) 1–9.
[20] R. Day, M. Fuller, V.A. Schmidt, Hysteresis properties of titanomagnetites: grain-size and compositional dependence, Phys. Earth Planet. Inter. 13 (1997) 260–267.
[21] J.W. King, S.K. Banerjee, J. Marvin, O. Ozdemir, A comparison of different magnetic methods for determining the relative grain-size of magnetite in natural materials: some results from lake sediments, Earth Planet. Sci. Lett. 59 (1982) 404–419.
[22] J.W. King, S.K. Banerjee, J. Marvin, A new rock-magnetic approach to selecting sediments for geomagnetic paleointensity studies: application to paleointensity for the last 4000 years, J. Geophys. Res. 88 (1983) 5911–5921.
[23] P. Rochette, M. Jackson, C. Aubourg, Rock magnetism and the interpretation of anisotropy of susceptibility, Rev. Geophys. 30 (1992) 209–226.
[24] K. Schwehr, L. Tauxe, Characterization of soft-sediment deformation Detection of cryptoslumps using magnetic methods, Geology 31 (2003) 203–206.
[25] N. Thouveny, K.M. Creer, I. Blunk, Extension of the Lac du Bouchet palaeomagnetic record over the last 120,000 years, Earth Planet. Sci. Lett. 97 (1990) 140–161.
[26] T. Williams, N. Thouveny, K.M. Creer, A normalised intensity record from Lac du Bouchet: geomagnetic paleointensity for the last 300 ka?, Earth Planet. Sci. Lett. 156 (1998) 33–46.
[27] L. Tauxe, Sedimentary records of relative paleointensity of the geomagnetic field: theory and practice, Rev. Geophys. 31 (1993) 319–354.
[28] N. Sigiura, ARM, TRM and magnetic interactions: concentration dependence, Earth Planet. Sci. Lett. 42 (1979) 451–455.
[29] T. Nishitani, M. Kono, Effect of low temperature oxidation on the remanence properties of titanomagnetites, J. Geomagn. Geoelectr. 41 (1989) 19–38.
[30] L. Tauxe, T. Pick, Y. Kok, Relative paleointensity in sediments: a pseudo-Thellier approach, Geophys. Res. Lett. 22 (1995) 2885–2888.
[31] J.P. Valet, L. Meynadier, A comparison of different techniques for relative paleointensity, Geophys. Res. Lett. 25 (1998) 89–92.
[32] L. Tauxe, G. Wu, Normalized remanence in sediments of the western equatorial pacific: relative paleointensity of the geomagnetic field?, J. Geophys. Res. 95 (1990) 12337–12350.
[33] W.S. Cleveland, S.J. Devlin, Locally weighted regression: an approach to regression analysis by local fitting, J. Am. Stat. Assoc. 403 (1988) 596–610.
[34] Y.S. Kok, L. Tauxe, Long-τ VRM and relative paleointensity estimates in sediments, Earth Planet. Sci. Lett. 168 (1999) 145–158.
[35] J.P. Valet, Time variations in geomagnetic intensity, Rev. Geophys. 41 (2003) 1–44.
[36] L. Tauxe, J.J. Love, Paleointensity in Hawaïan Scientific Drilling Project Hole (HSDP2): Results from submarine basaltic glass, Geochemist. Geophys. Geosyst. 4 (2003) 8702, doi:10.1029/2001GC000276.
[37] J.S. Gee, S.C. Cande, J.A. Hildebrand, K. Donnelly, R.L. Parker, Geomagnetic intensity variations over the past 780 kyr obtained from nea-seafloor anomalies, Nature 408 (2000) 827–832.
[38] M. McElhinny, W.E. Senanayake, Variations in the geomagnetic dipole 1. The past 50,000 years, J. Geomagn. Geoelectr. 34 (1982) 39–51.
[39] S. Yang, H. Odah, J. Shaw, Variations in the geomagnetic dipole moment over the last 12,000 years, Geophys. J. Int. 140 (2000) 158–162.
[40] N. Teanby, C. Laj, D. Gubbins, M. Pringle, A detailed paleointensity and inclination record from drill core SOH1 on Hawaii, Phys. Earth Planet. Inter. 131 (2002) 101–140.
[41] J.E.T. Channel, Geomagnetic paleointensity and directional secular variation at Ocean Drilling Program (ODP) site 984 (Bjorn drift) since 500 ka: comparison with ODP site 983 (Gardar drift), J. Geophys. Res. 104 (1999) 22937–22951.
[42] E. Tric, C. Laj, J.P. Valet, P. Tucholka, M. Paterne, F. Guichard, The Blake geomagnetic event: transition geometry, dynamical characteristics and geomagnetic significance, Earth Planet. Sci. Lett. 102 (1991) 1–13.
[43] N. Bonhommet, J. Babkine, Sur la présence d'aimantations inverses dans la Chaîne des Puys-Massif Central, France, C.R. Acad. Sci. Paris 264 (1967) 92.
[44] P. Vlag, N. Thouveny, D. Williamson, P. Rochette, F. Ben-Atig, Evidence for a geomagnetic excursion recorded in the sediments of Lac St. Front, France: A link with the Laschamp excursion?, J. Geophys. Res. 101 (1996) 28211–28230.
[45] P. Vlag, N. Thouveny, P. Rochette, Synthetic and sedimentary records of geomagnetic excursions, Geophys. Res. Lett. 24 (1997) 723–726.
[46] R.S. Coe, J.C. Liddicoat, Overprinting of natural magnetic remanence in lake sediments by subsequent high intensity field, Nature 367 (1994) 57–59.
[47] D. Kent, S.R. Hemming, B.D. Turrin, Laschamp excur-

sion at Mono lake?, Earth Planet. Sci. Lett. 6121 (2002) 1–14.
[48] J. Peck, J.W. King, S.M. Colman, V.A. Kravchinsky, An 84 kyr paleomagnetic record from the sediments of Lake Baikal, Siberia, J. Geophys. Res. 101 (1996) 11365–11385.
[49] K.M. Creer, P. Readman, A.M. Jacobs, Palaeomagnetic and paleontological dating of a section at Gioia Tauro, Italy: identification of the Blake event, Earth Planet. Sci. Lett. 50 (1980) 289–300.
[50] X.M. Fang, J.J. Li, R. Van der Voo, C. Mac Niocaill, X.R. Dai, R.A. Kemp, E. Derbyshire, J.-X. Cao, J.-M. Wang, G. Wang, A record of the Blake event during the last interglacial paleosol in the western plateau of China, Earth Planet. Sci. Lett. 146 (1997) 73–82.
[51] H. Oda, K. Nakamura, K. Ikehara, T. Nakano, M. Nishimura, O. Khlystov, Paleomagnetic record from Academician ridge, Lake Baikal: a reversal excursion at the base of marine oxygen isotope stage 6, Earth Planet. Sci. Lett. 202 (2002) 117–132.
[52] E. Herrero-Bervera, C.E. Helsley, A.M. Sarna-Wojcicki, K.R. Lajoie, C.E. Meyer, M.O. McWilliams, R.M. Negrini, B.D. Turrin, J.M. Donnelly-Nolan, J.C. Liddicoat, Age and correlation of a paleomagnetic episode in the western united states by Ar-40/Ar-39 dating and tephrochronology: the Jamaica, Blake or a new polarity episode?, J. Geophys. Res. 99 (1994) 24091–24103.
[53] P. Shane, T. Black, J. Westgate, Isothermal plateau fission-track age for a paleomagnetic excursion in the Mamaku ignimbrite, New Zealand and implication for late Quaternary stratigraphy, Geophys. Res. Lett. 21 (1994) 1695–1698.
[54] M. McWilliams, Global correlation of the 223 ka Pringle Falls Event, Int. Geol. Rev. 43 (2001) 191–195.
[55] C. Langereis, M.J. Dekkers, G.J. de Lange, M. Paterne, P.J.M. van Santvoort, Magnetostratigraphy and astronomical calibration of the last 1.1 Myr from an Eastern Mediterranean piston core and dating of short events in the Brunhes, J. Geophys. Res. 129 (2000) 75–94.
[56] N. Kawai, K. Yaskawa, T. Nakajima, M. Torii, S. Horie, Oscillating geomagnetic field with a recurring reversal discovered from lake Biwa, Proc. Jpn. Acad. 48 (1972) 186–190.
[57] S. Roger, J.L. Beaulieu, G. Féraud, N. Thouveny, M. Reille, C. Coulon, T. Williams, V. Andrieu, Ar/Ar dating of tephra of the Velay Maars: implications for paleoclimatic land-sea correlation, Earth Planet. Sci. Lett. 170 (1999) 287–299.
[58] D. Kent, J. Carlut, A negative test of orbital control of geomagnetic reversals and excursions, Geophys. Res. Lett. 28 (2001) 3561–3564.
[59] Y. Yokoyama, T. Yamazaki, Geomagnetic paleointensity variation with a 100 kyr quasi-period, Earth Planet. Sci. Lett. 181 (2000) 7–14.
[60] T. Yamazaki, H. Oda, Orbital influence on Earth's magnetic field 100,000-year periodicity in inclination, Science 295 (2002) 2435–2438.
[61] F.C. Bassinot, L.D. Labeyrie, E. Vincent, X. Quidelleur, N.J. Shackleton, Y. Lancelot, Astronomical theory of climate and the age of the Brunhes-Matuyama reversal, Earth Planet. Sci. Lett. 16 (1995) 91–108.
[62] D. Paillard, L. Labeyrie, P. Yiou, MacIntosh program performs time series analysis, EOS Trans. AGU 77 (1996) 379.